Chinese Journal of Natural Medicines

Discovery of antitumor diterpenoids from *Casearia graveolens* targeting VEGFR-2 to inhibit angiogenesis

Sibei WANG, Yuhui LIU, Yue LIANG, Yaru XI, Yupeng ZHAI, Dongho LEE, Jing XU, Yuanqiang GUO

Citation: Sibei WANG, Yuhui LIU, Yue LIANG, Yaru XI, Yupeng ZHAI, Dongho LEE, Jing XU, Yuanqiang GUO, Discovery of antitumor diterpenoids from *Casearia graveolens* targeting VEGFR-2 to inhibit angiogenesis, Chinese Journal of Natural Medicines, 2024, 22(9), 842-853. doi: 10.1016/S1875-5364(24)60566-2.

View online: https://doi.org/10.1016/S1875-5364(24)60566-2

Available online at www.sciencedirect.com
ScienceDirect
Chinese Journal of Natural Medicines 2024, **22**(9): 842-853
doi: 10.1016/S1875-5364(24)60566-2
Chinese Journal of Natural Medicines

•Original article•

Discovery of antitumor diterpenoids from *Casearia graveolens* targeting VEGFR-2 to inhibit angiogenesis

WANG Sibei[1Δ], LIU Yuhui[1Δ], LIANG Yue[1Δ], XI Yaru[1Δ], ZHAI Yupeng[1], LEE Dongho[3], XU Jing[1, 2*], GUO Yuanqiang[1*]

[1] *State Key Laboratory of Medicinal Chemical Biology, College of Pharmacy, and Tianjin Key Laboratory of Molecular Drug Research, Nankai University, Tianjin 300350, China;*
[2] *State Key Laboratory of Functions and Applications of Medicinal Plants, Guizhou Medical University, Guiyang 550014, China;*
[3] *Department of Plant Biotechnology, College of Life Sciences and Biotechnology, Korea University, Seoul 02841, South Korea*

Available online 20 Sep., 2024

[ABSTRACT] Eight novel clerodane diterpenoids (**1**−**8**) were isolated from the twigs of *Casearia graveolens*. Their structures were elucidated through comprehensive nuclear magnetic resonance (NMR), high-resolution electrospray ionization mass spectrometry (HR-ESI-MS), and electronic circular dichroism (ECD) analyses. In addition to structural determination, surface plasmon resonance (SPR) assays were conducted to investigate molecular interactions, revealing that compound **8** exhibited high affinity for vascular endothelial growth factor receptor 2 (VEGFR2), a key regulator of tumor angiogenesis. Subsequent *in vivo* experiments demonstrated that compound **8** effectively inhibited angiogenesis and displayed significant antitumor activity by suppressing tumor proliferation and metastasis in zebrafish xenograft models. These findings suggest that compound **8** holds promise as an anticancer lead compound targeting VEGFR-2 to obstruct tumor angiogenesis.

[KEY WORDS] Clerodane diterpenoids; *Casearia graveolens*; Surface plasmon resonance; Vascular endothelial growth factor receptor 2; Antitumor activity; Zebrafish

[CLC Number] R284, R965 **[Document code]** A **[Article ID]** 2095-6975(2024)09-0842-12

Introduction

Malignant tumors represent a significant threat to human health and life. Tumor biology research has revealed that tumor formation is closely linked to angiogenesis, the process by which new blood vessels form within the tumor microenvironment [1]. These new vessels provide essential oxygen and nutrients, facilitating tumor growth and metastasis. Angiogenesis is primarily driven by vascular endothelial growth factor (VEGF) and its receptors (VEGFRs) [2, 3], with VEGFR-2 playing a critical role in tumor initiation, progression, and metastasis. Targeting VEGFR-2 or its signaling pathways can inhibit angiogenesis, thereby suppressing tumor growth and spread [4]. Consequently, VEGFR-2 has emerged as a key target for the development of novel antitumor therapies.

Natural products have long been a cornerstone in drug discovery and development [5, 6]. Among these, diterpenoids are a notable class of natural compounds characterized by diverse structures and a wide range of biological activities. The genus *Casearia*, part of the Salicaceae family, includes approximately 180 species worldwide [7], with several species found in Yunnan and Hainan Provinces, China [8]. Historically, *Casearia*, such as *C. flexuosa*, *C. glomerata*, and *C. kurzii* have been used in traditional medicine to treat wounds, burns, rashes, eczema, and vitiligo. Chemical studies of species like *C. nigrescens* [9], *C. kurzii* [10], *C. sylvestris* [11, 12], *C. grewiifolia* [13], *C. lucida* [14], *C. guianensis* [15], and *C. graveolens* [16] have identified a rich array of natural products with various biological activities. *C. graveolens* Dalzell, a tropical tree primarily found in the wet regions of Yunnan Province, China, has been noted for its rich diterpenoid content, some of which exhibit significant cytotoxicity [17-19]. In our ongoing quest for potential lead compounds targeting VEGFR-2 to combat malignant tumors, we investigated the chemical constituents of *C. graveolens* twigs. This investigation led to the

[Received on] 25-Jan.-2024
[Research funding] This work was supported by the National Natural Science Foundation of China (No. 22077067), the Project of State Key Laboratory of Functions and Applications of Medicinal Plants, Guizhou Medical University [No. QJJ(2022)422], and the 111 Project (No. B20016).
[*]**Corresponding author]** E-mails: xujing611@nankai.edu.cn (XU Jing); victgyq@nankai.edu.cn (GUO Yuanqiang)
[Δ]These authors contributed equally to this work.
These authors have no conflict of interest to declare.

isolation of eight new clerodane-type diterpenoids, named caseaveolens A−H (**1**−**8**) (Fig. 1), from the methanolic extract of *C. graveolens*. The structures of these compounds were elucidated through extensive spectroscopic analyses. Surface plasmon resonance (SPR) experiments were conducted to assess the interactions between these compounds and VEGFR-2. Given the crucial role of VEGFR-2 in angiogenesis, the *in vivo* anti-angiogenic activity of these compounds was evaluated using transgenic zebrafish models. Further, the *in vivo* antitumor activity of the most potent anti-angiogenic compound was assessed in tumor-bearing zebrafish.

Results and Discussion

Structure elucidation

Compound **1** was obtained as a colorless oil. High-resolution electrospray ionization mass spectrometry (HR-ESI-MS) suggested a molecular formula of $C_{29}H_{44}O_7$, indicated by a peak at *m/z* 527.2988 $[M + Na]^+$ (Calcd. for $C_{29}H_{44}NaO_7$, 527.2985), corresponding to eight degrees of unsaturation. The infrared (IR) spectrum exhibited absorption bands for carbonyl groups (1751 and 1731 cm^{-1}) and double bonds (1653 and 1636 cm^{-1}). The ^1H nuclear magnetic resonance (NMR) spectrum showed signals corresponding to seven methyl groups [δ_H 2.03 (3H, s), 1.95 (3H, s), 1.65 (3H, s), 1.14 (3H, d, J = 7.0 Hz), 0.91 (3H, t, J = 7.5 Hz), 0.87 (3H, d, J = 6.8 Hz), and 0.85 (3H, s)], four olefinic protons [δ_H 6.33 (1H, dd, J = 17.4, 10.7 Hz), 5.40 (1H, dd, J = 6.8, 4.6 Hz), 5.08 (1H, d, J = 17.4 Hz), and 4.92 (1H, d, J = 10.7 Hz)], and three oxymethine protons [δ_H 6.46 (1H, d, J = 7.0 Hz), 6.20 (1H, s), and 5.24 (1H, m)]. The ^{13}C NMR spectrum displayed a total of 29 carbon signals. Analysis of the ^1H and ^{13}C NMR spectra indicated the presence of two acetyloxy groups, inferred from the methyl singlets (δ_H 1.95 and 2.03) and the corresponding carbonyl and methyl resonances (δ_C 169.8, 169.6, 21.5, and 21.1). Additionally, the proton and carbon signals (δ_H 2.33, 1.46, 1.68, 0.91, and 1.14; δ_C 176.5, 41.1, 26.7, 11.6, and 16.6) suggested the presence of a 2-methylbutyryloxy group, which was confirmed by heteronuclear multiple quantum coherence (HMQC) and heteronuclear multiple bond correlation (HMBC) spectra. The remaining 20 carbons in the ^{13}C NMR spectrum included four olefinic carbons (δ_C 141.3, 135.6, 129.2, and 110.7), two acetal carbons (δ_C 99.3 and 98.2), one oxygenated carbon (δ_C 69.9), and thirteen aliphatic carbons (δ_C 49.7, 46.6, 37.4, 37.1, 35.7, 33.1, 30.2, 27.4, 26.9, 26.7, 26.4, 15.5, and 11.9). Based on previously reported compounds from the *Casearia* species, these carbon signals and their chemical shifts suggested that compound **1** is a typical 18,19-acetal clerodane-type diterpenoid [20-22]. Further analysis of the 2D NMR data corroborated this structure, confirming the clerodane-type skeleton of compound **1** (Fig. 2). The locations of the substituent groups were determined from HMBCs. Key long-range correlations from H-2 (δ_H 5.24), H-18 (δ_H 6.46), and H-19 (δ_H 6.20) to the carbonyl carbons at δ_C 176.5, 169.6, and 169.8 verified that the two acetyloxy groups and the 2-methylbutyryloxy group are positioned at C-2, C-18, and C-19, respectively. Thus, the

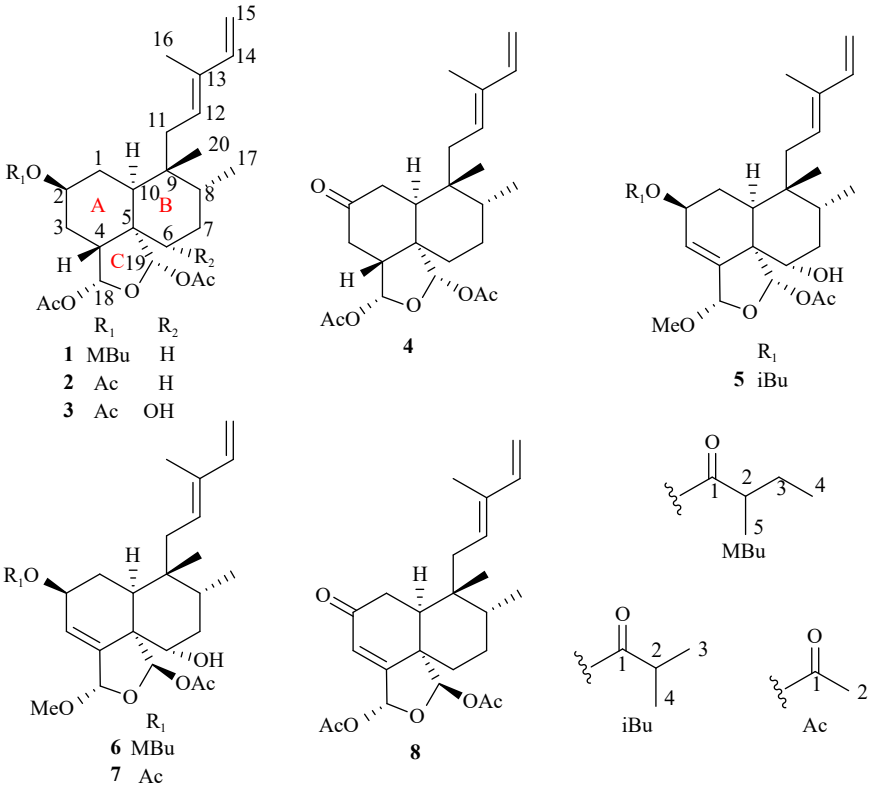

Fig. 1 Structures of compounds 1–8 from *C. graveolens*.

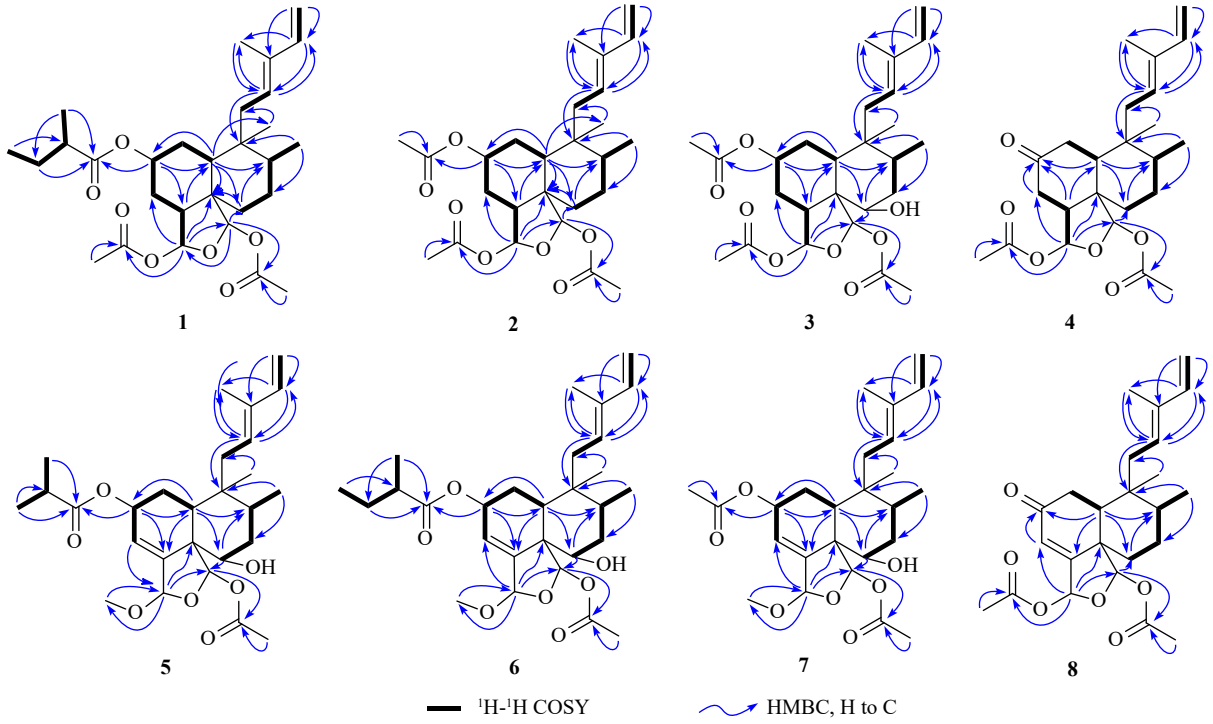

Fig. 2 ^{1}H–^{1}H COSY and key HMBCs of compounds 1–8.

planar structure of compound **1** was established as depicted.

The relative configuration of compound **1** was determined using nuclear Overhauser enhancement spectroscopy (NOESY). NOESY correlations revealed that the two six-membered rings were cis-fused, with both H-10 and C-19 in *α*-positions [18, 19]. Significant NOESY correlations were observed between H-2/H-10, H-10/H-11b, H-1*β*/H-6*β*, H-1*β*/Me-20, H-8/Me-20, H-4/H-6*β*, H-4/H-18, H-18/H-19, H-19/H-11a, H-11a/H-7*α*, and H-7*α*/Me-17. These findings, supported by Chem3D modeling, disclosed the conformation of compound **1** as depicted in Fig. 3. After establishing the relative configuration, the absolute configuration of compound **1** was determined using time-dependent density functional theory (TDDFT) electronic circular dichroism (ECD) calculations [23, 24]. The ECD spectrum was calculated at the CAM-B3LYP/SVP level using the conductor-like polarizable continuum (CPCM) model in acetonitrile. The calculated ECD spectrum (Fig. 4) closely matched the experimental data, suggesting an absolute configuration of (2*S*,4*R*,5*S*,8*R*,9*R*,10*S*, 18*R*,19*S*) for compound **1**.

The molecular formula of compound **2** was confirmed as $C_{26}H_{38}O_7$ based on high-resolution electrospray ionization mass spectrometry (HR-ESI-MS) data (*m/z* 485.2517 [M + Na]$^+$, Calcd. for $C_{26}H_{38}NaO_7$, 485.2515). Analysis of the ^{1}H and ^{13}C NMR spectra revealed the presence of three acetyloxy groups, indicated by signals at δ_H 1.94, 2.02, 2.03; δ_C 21.4, 21.3, 20.9, 169.5, 169.8, and 170.7. Comparisons with the NMR spectra of compound **1** indicated that compound **2** has the same 18,19-acetal skeleton. The 2D NMR spectra enabled the assignment of the skeletal proton and carbon signals. The oxygenated carbon, acetal carbons, and olefinic carbons forming two double bonds were identified as C-2 (δ_C 70.4), C-18 (δ_C 98.1), C-19 (δ_C 99.2), C-12 (δ_C 129.2), C-13 (δ_C 135.6), C-14 (δ_C 141.2), and C-15 (δ_C 110.6). The three acetyloxy groups were located at C-2, C-18, and C-19, as confirmed by HMBCs of H-2, H-18, and H-19 to the corresponding carbonyl carbons at δ_C 170.7, 169.8, and 169.5, respectively. Thus, the 2D structure of compound **2** was established. NOESY revealed cross-peaks between H-2/H-10, H-10/H-11b, H-1*β*/H-6*β*, H-1*β*/Me-20, H-8/Me-20, H-4/H-6*β*, H-4/H-18, H-18/H-19, H-19/H-11a, H-11a/H-7*α*, and H-7*α*/Me-17. These correlations indicated that H-2, H-10, and Me-17 were *α*-oriented, while H-4, H-8, H-18, H-19, and Me-20 were *β*-oriented. Consequently, compound **2** was inferred to have the same relative configuration as compound **1**. The absolute configuration of compound **2** was determined as 2*S*, 4*R*, 5*S*, 8*R*, 9*R*, 10*S*, 18*R*, and 19*S* by comparing the experimental and calculated ECD spectra (Fig. 4).

The molecular formula of compound **3** was determined to be $C_{26}H_{38}O_8$ based on HR-ESI-MS data (*m/z* 501.2462 [M + Na]$^+$, Calcd. for $C_{26}H_{38}NaO_8$, 501.2464). The ^{1}H and ^{13}C NMR spectra of compound **3** were similar to those of compound **2**, suggesting that compound **3** has a typical 18,19-acetal clerodane-type diterpenoid structure with three acetyloxy groups (Tables 1 and 2). The primary difference between compounds **2** and **3** was the presence of an additional oxygenated carbon (δ_C 74.6) in compound **3**, which replaced a methylene aliphatic carbon present in compound **2**. Further 2D NMR experiments indicated that the methylene carbon (δ_C 33.0) in compound **2** was replaced by the oxygenated carbon (δ_C 74.6) in compound **3**. HMBCs from δ_H 5.28 (H-2), 6.50 (H-18), and 6.35 (H-19) to carbonyl carbons at δ_C

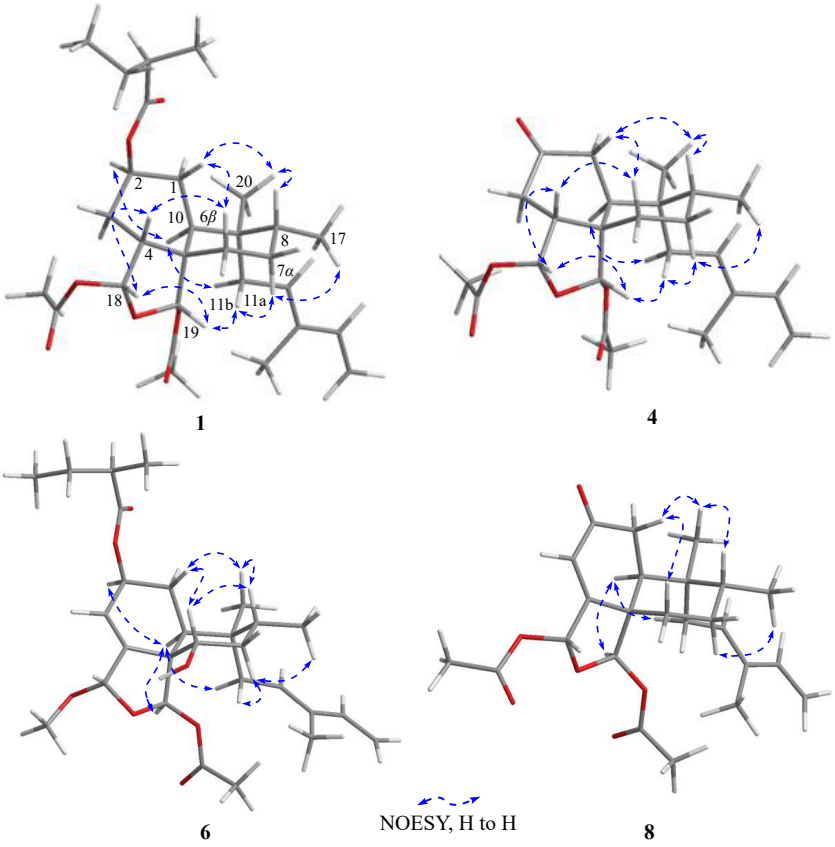

Fig. 3 Key NOESY correlations of compounds 1, 4, 6, and 8.

170.8, 169.3, and 169.7, respectively, confirmed the positions of the three acetyloxy groups at C-2, C-18, and C-19. The relative configuration of compound **3** was established using the NOESY spectrum and Chem3D molecular modeling. The absolute configuration of compound **3** was determined through ECD calculations, which closely matched the experimental data, confirming the configuration as 2*S*, 4*R*, 5*S*, 6*S*,8*R*, 9*R*, 10*S*, 18*R*, and 19*S*.

The molecular formula of compound **4** was determined as $C_{24}H_{34}O_6$ based on HR-ESI-MS data, which showed an ion at *m/z* 419.2434 $[M + H]^+$ (Calcd. for $C_{24}H_{35}O_6$, 419.2434). The ^1H and ^{13}C NMR spectra revealed signals corresponding to two acetyloxy groups (δ_H 2.04 and 1.96; δ_C 21.0, 21.5, 169.4, and 169.5), along with characteristic olefinic carbon resonances (δ_C 128.5, 136.1, 141.1, and 111.1) and two acetal carbons (δ_C 99.1 and 97.3). These features indicated that compound **4** is an 18,19-acetal clerodane-type diterpenoid, similar to compounds **1**−**3**. Comparing the chemical shifts of compound **4** with those of compound **1** revealed that an oxygenated carbon in compound **1** was replaced by a ketone carbonyl carbon (δ_C 212.5) in compound **4**. Interpretation of the 1D and 2D NMR spectra assigned this ketone carbonyl carbon to C-2, and the other skeletal proton and carbon signals were also attributed accordingly (Tables 1 and 2). The positions of the two acetyloxy groups were confirmed by HMBCs from H-18 and H-19 to the ester carbonyl carbons at δ_C 169.4 (C-18) and 169.5 (C-19), respectively. NOESY correlations revealed interactions between H-10/H-11b, H-1*β*/H-6*β*, H-1*β*/Me-20, H-8/Me-20, H-4/H-6*β*, H-4/H-18, H-18/H-19, H-19/H-11a, H-11a/H-7*α*, and H-7*α*/Me-17. These correlations suggested that H-4, H-8, H-18, H-19, and Me-20 were *β*-oriented, while H-10, Me-17, and C-19 were in *α*-oriented. The calculated ECD spectrum of compound **4** closely matched the experimental data (Fig. 4), confirming an absolute configuration of 4*R*, 5*S*, 8*R*, 9*R*, 10*S*, 18*R*, and 19*S*.

The molecular formula of **5** was determined to be $C_{27}H_{40}O_7$ based on HR-ESI-MS data (*m/z* 499.2672 $[M + Na]^+$, Calcd. for $C_{27}H_{40}NaO_7$, 499.2672). The ^1H and ^{13}C NMR spectra were similar to those of compounds **1**−**4**, indicating that compound **5** is also an 18,19-acetal clerodane diterpenoid. In addition to a methoxy group (δ_H 3.43; δ_C 56.2), the presence of isobutyryloxy and acetyloxy groups was confirmed from the corresponding proton and carbon signals (Tables 1 and 2). The ^{13}C NMR spectrum of compound **5** revealed two acetal carbons (δ_C 104.3 and 96.4), two oxygenated carbons (δ_C 74.2 and 70.6), and six olefinic carbons (δ_C 145.2, 141.3, 135.6, 129.1, 123.9, and 111.0). The presence of two additional olefinic carbons, compared to compounds **1**−**4**, indicated the positions of C-3 and C-4, as determined by 2D NMR spectra analysis. The remaining carbon and proton signals were also assigned through detailed analysis of 1D and 2D NMR data. HMBCs identified the positions of the isobutyryloxy, methoxy, and acetyloxy groups, linking them to C-2, C-18, and C-19, respectively. Specifically, correla-

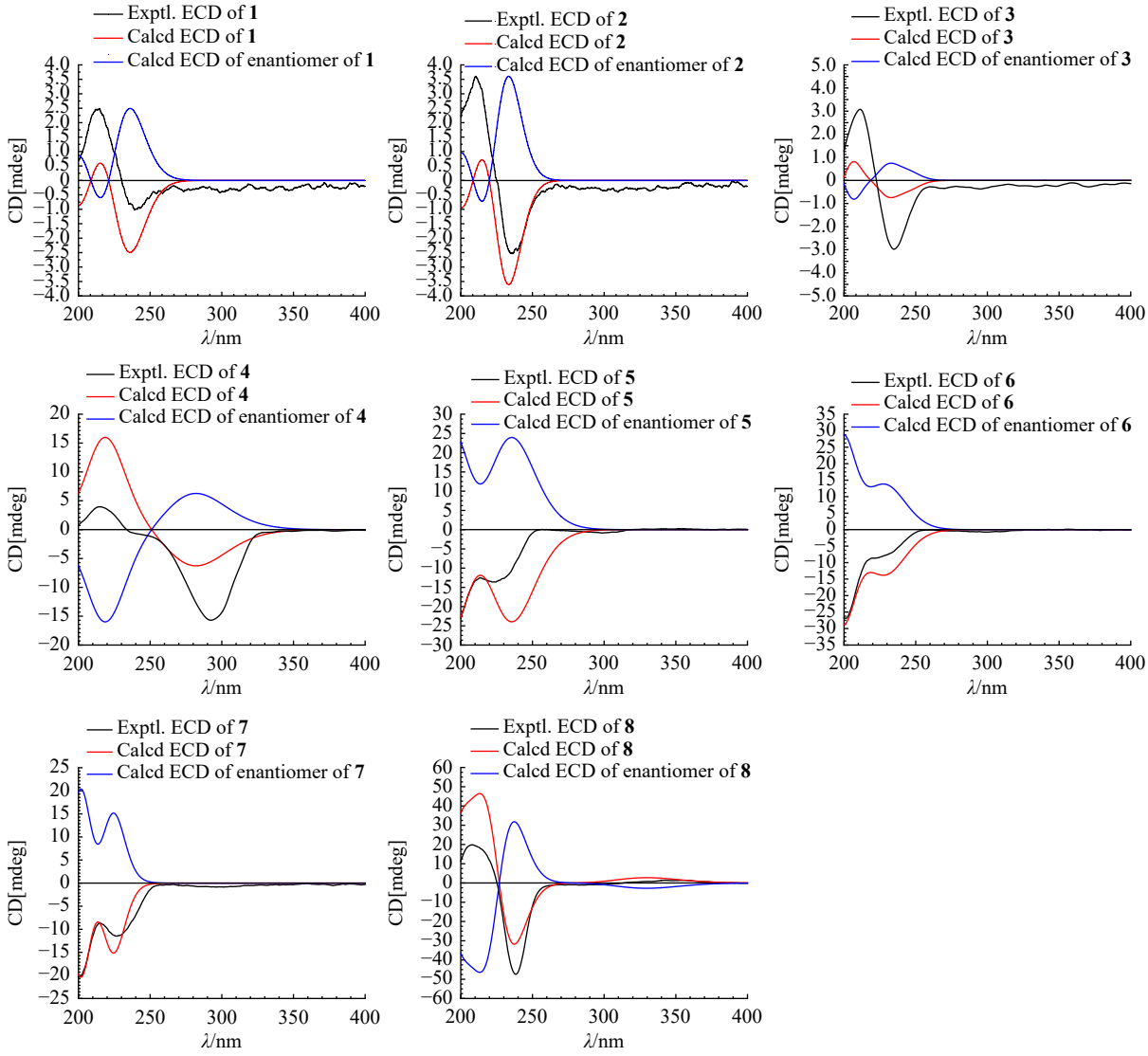

Fig. 4 Calculated and experimental ECD spectra of compounds 1–8 in acetonitrile.

tions from H-2, H-18, and H-19 to the carbon signals at δ_C 176.8, 56.2, and 170.0 confirmed these linkages (Fig. 2). The relative configuration of compound **5** was established based on its NOESY spectrum. The absolute configuration was further confirmed as 2*S*, 5*S*, 6*S*, 8*R*, 9*R*, 10*S*, 18*S*, and 19*S* by comparing the calculated and experimental ECD spectra.

Compounds **6** and **7** were determined to have the same structural scaffold as compound **5**, as evidenced by characteristic NMR signals for six olefinic carbons, two acetal carbons, and two oxygenated carbons (Tables 1 and 2). The primary differences between these compounds were their substituent groups. In addition to the common acetyloxy and methoxy groups, compound **6** featured a 2-methylbutyryloxy group (δ_H 0.92, 1.16, 1.48, 1.73, and 2.38; δ_C 11.7, 16.6, 26.8, 42.2, and 176.6) instead of the isobutyryloxy group present in compound **5**. Compound **7**, on the other hand, had an additional acetyloxy group in place of the isobutyryloxy group in compound **5**. The positions of these substituent groups were determined through long-range correlations in the HMBC spectra, as shown in Fig. 2. The relative configurations of compounds **6** and **7** were elucidated using NOESY correlations, which included H-1*β*/H-6*β*, H-1*β*/Me-20, H-8/Me-20, H-2/H-10, H-10/H-19, H-10/H-11b, H-11a/H-7*α*, and H-7*α*/Me-17. Notably, in compounds **6** and **7**, the acetyloxy group at C-19 was positioned on the *β*-side of the furan ring, in contrast to its *α*-orientation in compound **5**. This was confirmed by the correlations between H-19/H-2 and H-10. The absolute configurations of compounds **6** and **7** were determined by comparing experimental and calculated ECD spectra. Compound **6** was established to have the absolute configuration of 2*S*, 5*S*, 6*S*, 8*R*, 9*R*, 10*S*, 18*S*, and 19*R*. Similarly, compound **7** was determined to have the absolute configuration of 2*S*, 5*S*, 6*S*, 8*R*, 9*R*, 10*S*, 18*S*, and 19*R*.

Compound **8** was obtained as a colorless oil, with its molecular formula determined as $C_{24}H_{32}O_6$ based on HR-ESI-MS data (*m/z* 439.2091 $[M + Na]^+$, Calcd. for $C_{24}H_{32}NaO_6$, 439.2097). The ^1H and ^{13}C NMR spectra of compound **8** were similar to those of compound **4**. The key difference was the

Table 1 ^{13}C NMR Data for compounds 1–8 (δ in ppm, 100 MHz, in $CDCl_3$)

No.		1	2	3	4	5	6	7	8
1		26.9, CH_2	26.7, CH_2	27.2, CH_2	37.8, CH_2	26.2, CH_2	26.7, CH_2	26.7, CH_2	35.3, CH_2
2		69.9, CH	70.4, CH	70.1, CH	212.5, C	70.6, CH	70.6, CH	70.9, CH	199.1, C
3		26.7, CH_2	26.6, CH_2	26.3, CH_2	37.3, CH_2	123.9, CH	127.0, CH	126.6, CH	123.8, CH
4		46.6, CH	46.5, CH	43.6, CH	47.9, CH	145.2, C	144.7, C	145.0, C	165.3, C
5		49.7, C	49.7, C	54.5, C	49.4, C	53.4, C	51.8, C	51.7, C	50.2, C
6		33.1, CH_2	33.0, CH_2	74.6, CH	33.9, CH_2	74.2, CH	72.4, CH	72.4, CH	29.7, CH_2
7		27.4, CH_2	27.3, CH_2	36.9, CH_2	27.4, CH_2	37.7, CH_2	36.0, CH_2	36.0, CH_2	27.1, CH_2
8		37.1, CH	37.1, CH	37.5, CH	37.2, CH	36.7, CH	35.6, CH	35.6, CH	35.9, CH
9		37.4, C	37.3, C	37.6, C	37.4, C	38.4, C	38.4, C	38.4, C	37.9, C
10		35.7, CH	35.7, CH	37.0, CH	36.1, CH	41.4, CH	41.1, CH	42.2, CH	39.3, CH
11		30.2, CH_2	30.2, CH_2	30.2, CH_2	30.1, CH_2	30.1, CH_2	29.7, CH_2	29.7, CH_2	29.9, CH_2
12		129.2, CH	129.2, CH	128.9, CH	128.5, CH	129.1, CH	129.4, CH	129.4, CH	128.4, CH
13		135.6, C	135.6, C	135.8, C	136.1, C	135.6, C	135.5, C	135.5, C	136.1, C
14		141.3, CH	141.2, CH	141.1, CH	141.1, CH	141.3, CH	141.3, CH	141.3, CH	141.1, CH
15		110.7, CH_2	110.6, CH_2	111.0, CH_2	111.1, CH_2	111.0, CH_2	110.9, CH_2	111.0, CH_2	111.2, CH_2
16		11.9, CH_3	11.9, CH_3	12.0, CH_3	12.0, CH_3	11.9, CH_3	11.9, CH_3	11.9, CH_3	12.0, CH_3
17		15.5, CH_3	15.5, CH_3	15.5, CH_3	15.6, CH_3	15.6, CH_3	15.6, CH_3	15.6, CH_3	15.5, CH_3
18		98.2, CH	98.1, CH	98.9, CH	97.3, CH	104.3, CH	103.7, CH	103.8, CH	93.7, CH
19		99.3, CH	99.2, CH	97.5, CH	99.1, CH	96.4, CH	97.9, CH	97.9, CH	98.6, CH
20		26.4, CH_3	26.3, CH_3	25.6, CH_3	26.0, CH_3	25.1, CH_3	25.2, CH_3	25.2, CH_3	24.8, CH_3
OR-2[a]	1	176.5, C	170.7, C	170.8, C		176.8, C	176.6, C	170.9, C	
	2	41.1, CH	20.9, CH_3	21.0, CH_3		34.1, CH	42.2, CH	21.2, CH_3	
	3	26.7, CH_2				19.0, CH_3	26.8, CH_2		
	4	11.6, CH_3				19.0, CH_3	11.7, CH_3		
	5	16.6, CH_3					16.6, CH_3		
OR-18[a]	1	169.6, C	169.8, C	169.3, C	169.4, C	56.2, CH_3	56.1, CH_3	56.1, CH_3	169.8, C
	2	21.1, CH_3	21.3, CH_3	21.4, CH_3	21.0, CH_3				21.0, CH_3
OR-19[a]	1	169.8, C	169.5, C	169.7, C	169.5, C	170.0, C	169.6, C	169.6, C	169.4, C
	2	21.5, CH_3	21.4, CH_3	21.6, CH_3	21.5, CH_3	21.7, CH_3	21.8, CH_3	21.8, CH_3	21.4, CH_3

[a]A number with a superscript indicates the location of the substituent group in the parent skeleton.

presence of two additional olefinic carbons in compound **8** and a significant shift in the carbonyl carbon signal (δ_C 199.1 in **8** compared to δ_C 212.5 in **4**). This shift suggested that the carbonyl carbon in compound **8** was part of an *α*,*β*-unsaturated ketone, supported by the observed HMBCs. HMBCs provided further structural insights: H-10 correlated with δ_C 199.1 (C-2) and 165.3 (C-4), H-3 correlated with δ_C 199.1 (C-2), and H-18 correlated with δ_C 123.8 (C-3). These correlations confirmed the presence of the *α*,*β*-unsaturated ketone structure in compound **8**. The relative configuration of compound **8** was determined using NOESY, revealing a configuration similar to that of compounds **6** and **7**. The absolute configuration of compound **8** was established by comparing its calculated and experimental ECD spectra, both showing identical Cotton effects (CEs). This comparison confirmed the absolute configuration as (5*S*,8*R*,9*R*,10*S*,18*R*,19*R*).

SPR assay

VEGFR-2 plays a critical role in tumor angiogenesis and has become a focal point in drug development [4]. To evaluate the potential of the newly identified clerodane diterpenoids for anticancer therapy, we conducted a series of biological assays. These included surface plasmon resonance (SPR) experiments to examine interactions with VEGFR-2, as well as *in vivo* anti-angiogenesis activity assessments us-

Table 2 ^{1}H NMR Data for compounds **1**–**8** (δ in ppm, J in Hz, 400 MHz, in $CDCl_3$)

No.		1	2	3	4	5	6	7	8
1*a*		2.08 m	2.09 m	2.23 m	2.30 m[b]	2.16 m	2.11 m	2.13 m	2.52 m[b]
1*β*		1.26 m	1.30 m	1.30 m	2.46 m[b]	1.62 m	1.68 m	1.74 m	2.64 m[b]
2		5.24 m	5.25 m	5.28 m		5.58 t (8.4)	5.58 t (8.2)	5.57 m	
3*a*		2.23 m	2.28 m	2.08 m	2.76 t (15.4)	5.98 s	6.06 d (1.8)	6.09 s	6.08 s
3*β*		1.44 m	1.51 m	1.62 m	2.20 m[b]				
4		2.23 m	2.20 m	2.67 m	2.32 m[b]				
6*a*		1.74 m	1.74 m		1.85 m				1.84 m
6*β*		1.55 m	1.56 m	3.80 br d (11.1)	1.48 m	3.98 dd (12.1, 3.9)	4.10 dd (11.8, 4.2)	4.09 dd (11.9, 4.4)	1.65 m
7*a*		1.95 m	2.03 m	1.73 m	1.50 m	1.62 m	1.61 m	1.59 m	1.67 m
7*β*		1.36 m	1.38 m	1.56 m	1.45 m	1.77 m	1.80 m	1.77 m	1.54 m
8		1.55 m	1.53 m	2.08 m	1.52 m	1.84 m	1.92 m	1.90 m	1.72 m
10		1.90 d (13.8)	1.89 d (14.0)	1.73 m[b]	2.48 m[b]	2.39 dd (14.0, 2.5)	2.38 dd (13.8, 6.8)	2.25 m[b]	2.67 m[b]
11a		2.18 m[b]	2.17 m[b]	2.19 m[b]	2.22 m[b]	2.21 dd (17.1, 8.5)	2.22 dd (16.3, 8.4)	2.22 m[b]	2.24 dd (17.3, 8.1)
11b		1.73 m[b]	1.73 m[b]	1.64 m[b]	1.80 m[b]	1.68 m[b]	1.69 m[b]	1.64 m[b]	1.75 m[b]
12		5.40 dd (6.8, 4.6)	5.39 t (5.5)	5.35 m	5.39 t (5.3)	5.39 d (6.9)	5.36 d (6.9)	5.35 d (6.9)	5.39 m
14		6.33 dd (17.4, 10.7)	6.32 dd (17.4, 10.7)	6.31dd (17.3, 10.7)	6.32 dd (17.4, 10.7)	6.30 dd (17.3,10.6)	6.30 dd (17.4, 10.7)	6.30 dd (17.3,10.7)	6.30 dd (17.4, 10.6)
15a		4.92 d (10.7)	4.92 d (10.7)	4.94 d (10.7)	4.94 d (10.7)	4.93 d (10.6)	4.93 d (10.7)	4.93 d (10.7)	4.94 d (10.6)
15b		5.08 d (17.4)	5.08 d (17.4)	5.09 d (17.3)	5.10 d (17.4)	5.08 d (17.3)	5.08 d (17.4)	5.08 d (17.3)	5.10 d (17.4)
16		1.65 s	1.65 s	1.65 s	1.67 s	1.66 s	1.66 s	1.66 s	1.66 s
17		0.87 d (6.8)	0.88 d (7.2)	0.91 d (5.6)	0.90 d (6.3)	0.93 d (6.7)	0.93 d (6.3)	0.93 d (6.7)	0.93 d (6.7)
18		6.46 d (7.0)	6.45 d (6.9)	6.50 d (6.9)	6.49 d (7.1)	5.47 s	5.27 s	5.27 s	6.82 s
19		6.20 s	6.19 s	6.35 s	6.29 s	6.45 s	6.56 s	6.56 s	6.45 s
20		0.85 s	0.85 s	0.83 s	0.85 s	0.83 s	0.83 s	0.83 s	0.85 s
OR-2[a]	2	2.33 q (6.9)	2.03 s	2.04 s		2.55 m	2.38 m	2.09 s	
	3	1.46 m; 1.68 m				1.19 s	1.48 m; 1.73 m		
	4	0.91 t (7.5)				1.17 s	0.92 t (5.0)		
	5	1.14 d (7.0)					1.16 d (6.9)		
OR-18[a]	2	2.03 s	2.02 s	2.04 s	2. 04 s	3.43 s	3.49 s	3.50 s	2.11 s
OR-19[a]	2	1.95 s	1.94 s	1.94 s	1.96 s	1.95 s	1.92 s	1.92 s	1.95 s

[a]A number with a superscript indicates the location of the substituent group in the parent skeleton; [b]Signals were overlapped and the multiplicities could not be distinguished.

ing a transgenic zebrafish model. Before performing the SPR experiments, we assessed the cytotoxicity of these diterpenoids. As shown in Fig. 5A, compound **8** exhibited the most significant inhibitory effect on MCF-7 cells at a concentration of 10 μmol·L^{-1}. Based on these findings, compound **8** was selected for the SPR analysis. As shown in Fig. 5B, the SPR experiments revealed clear molecular interactions between compound **8** and VEGFR-2, with response signals increasing in a concentration-dependent manner. The SPR affinity assay demonstrated that compound **8** binds strongly to the VEGFR-2 protein, suggesting that it may inhibit angiogenesis by targeting VEGFR-2.

Molecular docking simulation

To further elucidate the molecular mechanism of the interaction between compound **8** and the VEGFR-2 target protein, molecular docking simulations were performed to model the binding pattern of compound **8** with VEGFR-2. As depicted in Fig. 6, the results indicated that the two acetyloxy groups of compound **8** formed hydrogen bonds with the amino acids Cys919 and Asn923. Additionally, compound **8** interacted with Leu840, Gly841, Gly846, Val848, Val916, Phe918, Gly922, Asn1033, Leu1035, and Asp1046 through

hydrophobic interactions. The binding free energy between compound **8** and VEGFR-2 was calculated to be –7.1 kcal·mol^{-1}. These molecular docking results suggest that compound **8** binds to the ATP-binding site of VEGFR-2 [4, 25], which could explain its mechanism of inhibiting angiogenesis by targeting this receptor.

In vivo antiangiogenetic activity of compound 8 in a transgenic zebrafish model

The SPR experiments and molecular docking analysis discovered that compound **8** could associate with the target protein VEGFR-2. VEGFR-2 plays an important role in regulating tumor angiogenesis [4]. To verify whether compound **8** can inhibit angiogenesis by targeting VEGFR-2, the *in vivo* antiangiogenetic effects of compound **8** were carried out using the transgenic zebrafish model, in which the vessels presented green fluorescence and were easily observed and quantified. After administrating compound **8** (0.25, 0.5, and 1 μmol·L^{-1}) and the positive drug (2 μmol·L^{-1}), the formation and development of the intersegmental vessels (ISVs) in zebrafish embryos were detected. From the results shown in Fig. 7, the intersegmental vessels of the zebrafish in the drug-treated group were lost and broken when compared with the control group. The quantification analysis showed that the average lengths in the zebrafish were 2888.80 ± 151.82 μm at 0.25 μmol·L^{-1}, 2437.54 ± 192.86 μm at 0.5 μmol·L^{-1}, and 1936.26 ± 119.79 μm at 1 μmol·L^{-1}, respectively, and the inhibitory effects on angiogenesis were dose-dependent. The angiogenetic experiments in the transgenic zebrafish suggested that compound **8** had the ability to target VEGFR-2 to suppress angiogenesis.

In vivo antitumor effects of compound 8 in tumor zebrafish xenografts

Angiogenesis plays a critical role in tumor progression, and its inhibition can effectively impede tumor growth [1, 26, 27]. Since compound **8** was shown to target VEGFR-2 and suppress angiogenesis, it was hypothesized that it might also possess antitumor properties. To test this hypothesis, we evaluated the antitumor activity of compound **8** using a tumor-bearing zebrafish model, created by microinjecting MCF-7 cells into the zebrafish yolk sac. As depicted in Fig. 8A, the relative intensity and foci of red fluorescence—which indicate tumor proliferation and metastasis [17]—were significantly inhibited in zebrafish treated with compound **8**. Quantification of the red fluorescence in zebrafish embryos using ImageJ software (Fig. 8B) showed a significant, dose-dependent reduction in both the total fluorescence intensity and the number of disseminated foci from the tumor mass. These results demonstrate that compound **8** effectively blocks tumor proliferation and metastasis *in vivo*, highlighting its potential as an antitumor agent.

Conclusions

This phytochemical study on the twigs of *Casearia graveolens* resulted in the isolation of eight new clerodane diterpenoids, named caseaveolen A–H (**1**–**8**). Their structures were elucidated using comprehensive 1D and 2D NMR spectroscopic analyses, and their absolute configurations were determined by comparing experimental and calculated ECD

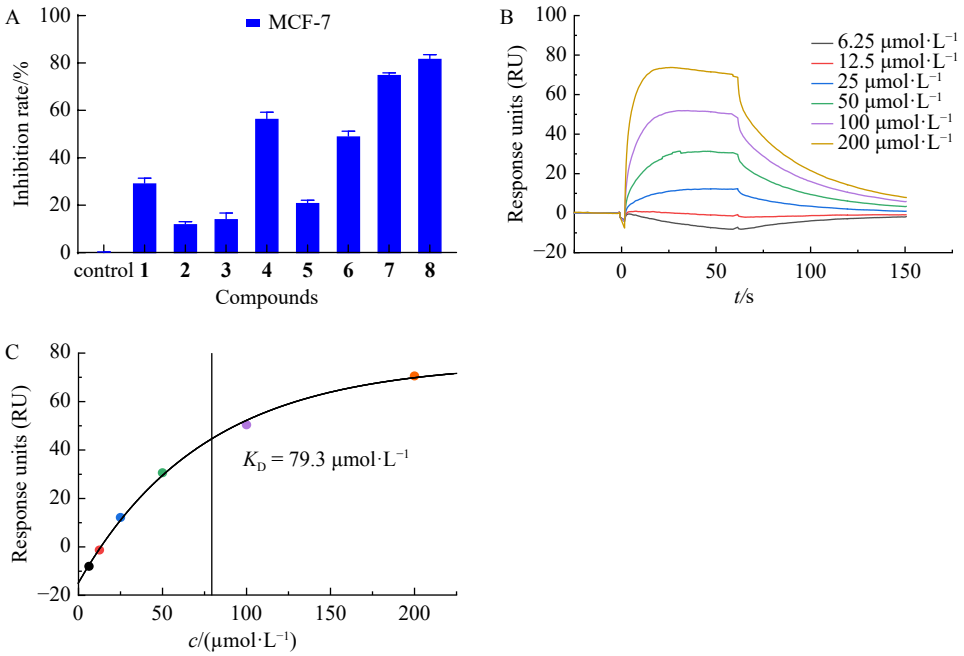

Fig. 5 (A) Proliferation inhibition rate of compounds 1–8 in MCF-7 cells by MTT assay. The inhibition rates are presented as the means ± SD (n = 3). (B) Affinities of compound 8 towards the VEGFR-2 protein by surface plasmon resonance assay. Sensorgrams were obtained by using different concentrations of compound 8 (6.25, 12.5, 25, 50, 100, and 200 μmol·L^{-1}). (C) The equilibrium binding constant (affinity, K_D) between compound 8 and VEGFR-2 was obtained using the fitting tool of the BIA evaluation software.

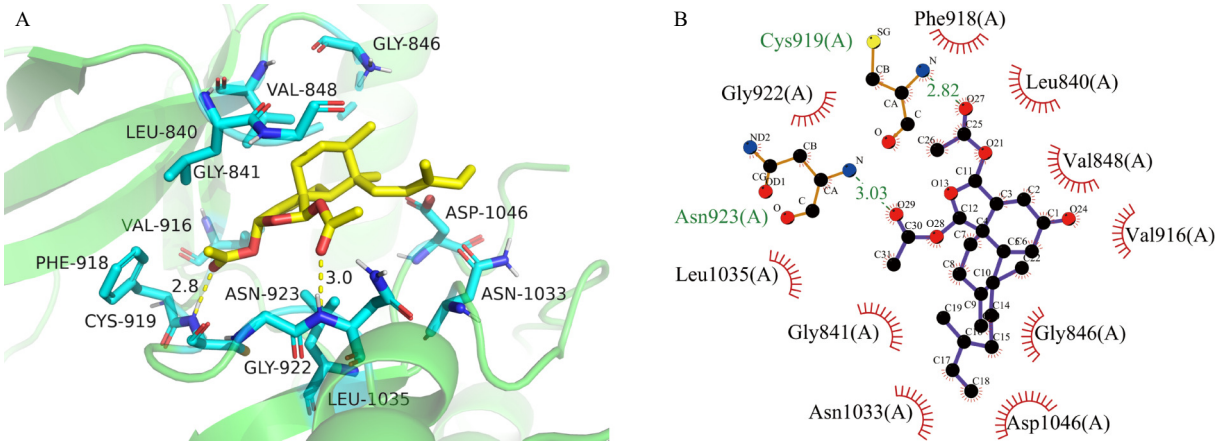

Fig. 6 Binding mode of compound 8 within the VEGFR-2 active site. (A) Molecular interactions and three-dimensional representations of hydrogen bonds and hydrophobic interactions of compound 8 with the VEGFR-2 receptor protein using PyMOL. The ligand is colored and represented in yellow; hydrogen bonds are displayed in yellow with dotted lines. (B) Molecular interactions and two-dimensional representations of hydrogen bonds and hydrophobic interactions of compound 8 with the VEGFR-2 receptor protein using LigPlot. The ligand is represented in a purple color; hydrogen bonds are displayed as green dotted lines, and red stellations represent hydrophobic interactions.

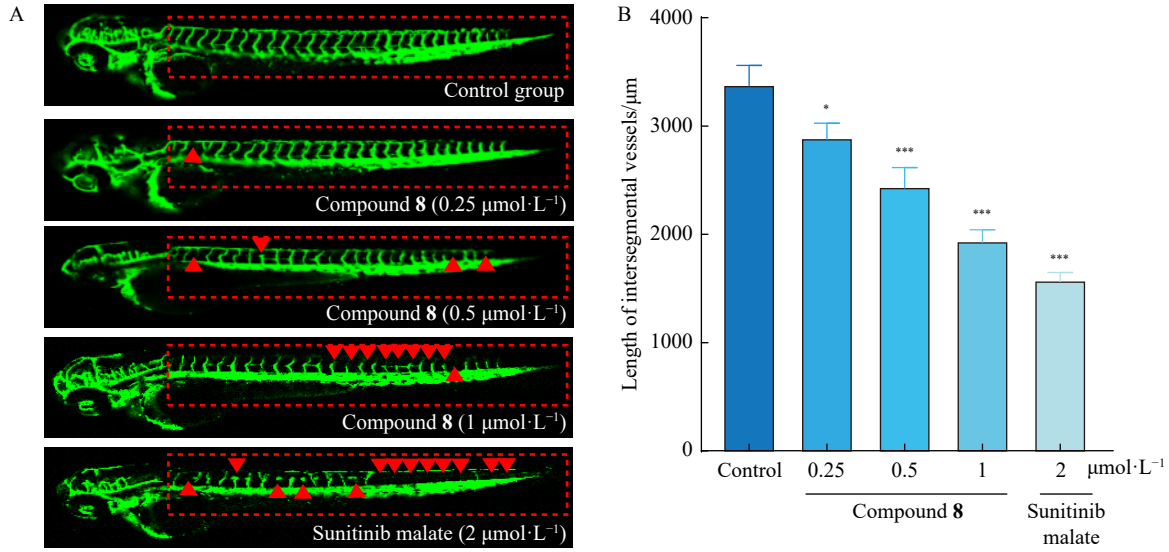

Fig. 7 The antiangiogenetic activity of compound 8 in a transgenic zebrafish model. (A) The development of intersegmental vessels (ISVs) at 48 hpf. Interrupted ISVs were indicated by red arrows. (B) Length of ISVs measured using Image J software. Each experiment was repeated three times, and the results are expressed as mean ± SD. $^{*}P < 0.05$, $^{***}P < 0.001$ *vs* the control group.

spectra. Additionally, surface plasmon resonance (SPR) experiments demonstrated that compound **8** has a strong affinity for VEGFR-2, a crucial target in the regulation of tumor angiogenesis. Molecular docking simulations indicated that compound **8** forms hydrogen bonds and hydrophobic interactions at the active site of the VEGFR-2 receptor. *In vivo* antiangiogenetic experiments, compound **8** effectively inhibited angiogenesis. Moreover, compound **8** displayed significant antitumor activity by suppressing tumor proliferation and metastasis in zebrafish xenografts. In conclusion, this study expands the structural diversity of natural clerodane diterpenoids and identifies compound **8** as a promising anticancer lead compound that targets VEGFR-2 to inhibit tumor angiogenesis.

Experimental

General experimental procedures

The instruments used to obtain spectroscopic data, including NMR, IR, ECD, optical rotation, and HR-ESI-MS, were the same as those described in our previous publications [10, 19]. All other materials and methods employed followed the protocols outlined in these references.

Plant material

The twigs of *Casearia graveolens* were collected in May 2015 from Xishuangbanna County, Yunnan Province, China. The botanical identification was conducted by one of the authors, GUO Yuanqiang. A voucher specimen (No. 20150509B) from this collection has been deposited in the Laboratory of Natural Medicines at Nankai University.

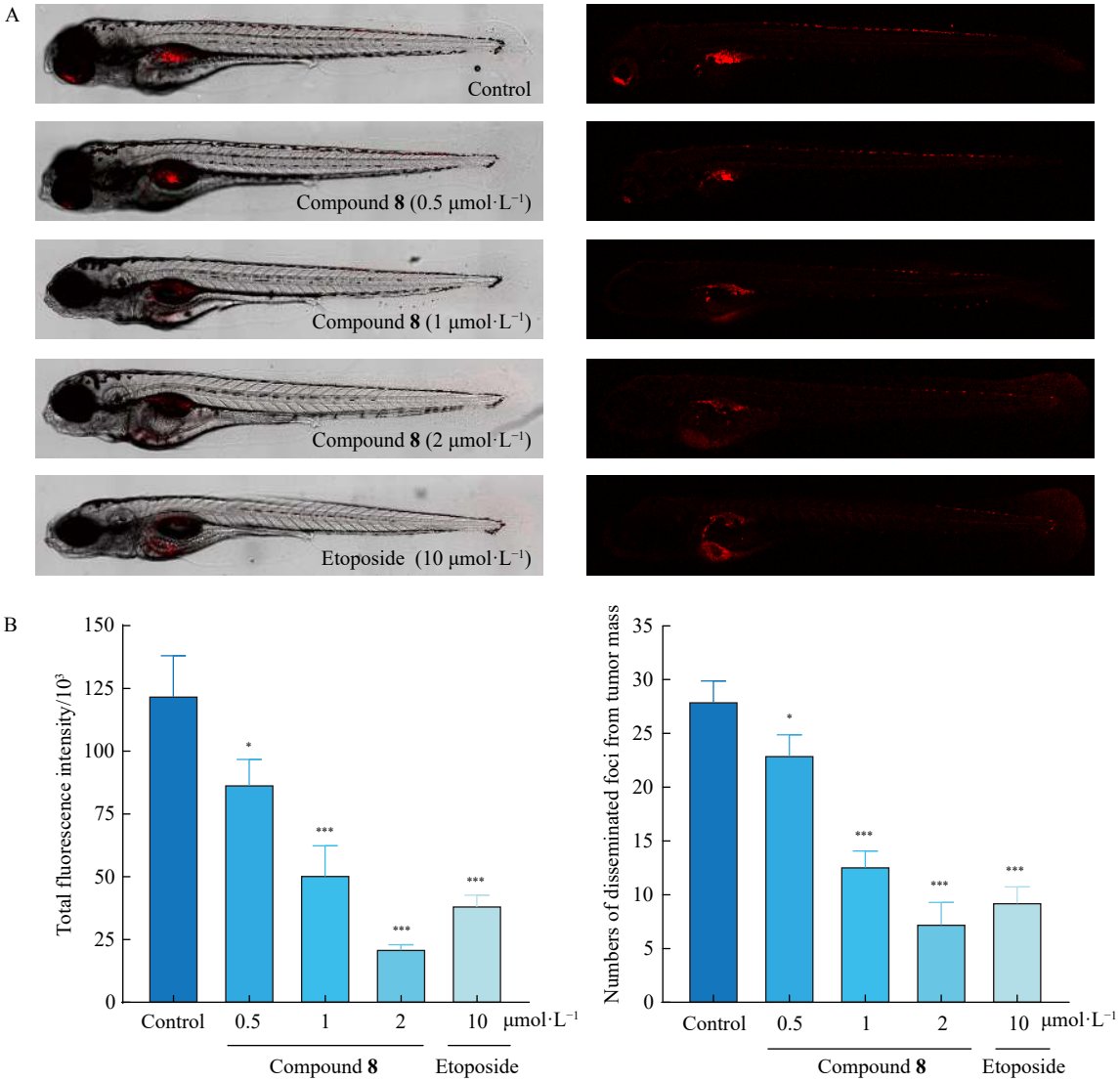

Fig. 8 ***In vivo*** **antitumor effects of compound 8 in a zebrafish xenograft model. (A) Representative images of the relative intensity and distribution of the red fluorescence in zebrafish embryos under a confocal microscope. (B) Total fluorescence intensity and numbers of disseminated foci from the tumor mass quantified using Image J software. Each experiment was repeated three times, and the results are expressed as mean ± SD.** $^{*}P < 0.05$, $^{***}P < 0.001$ ***vs*** **the control group.**

Extraction and isolation

The twigs of *Casearia graveolens* (30.0 kg) were cut into pieces and dried. The dried twigs were extracted with methanol (MeOH) (3 × 60 L) under reflux. The organic solvent was then evaporated, yielding a crude extract (1500 g). This extract was suspended in water (1.5 L) and partitioned with petroleum ether (5 × 1.5 L) and ethyl acetate (5 × 1.5 L). The ethyl acetate-soluble portion (105.5 g) was subjected to silica gel column chromatography (silica gel, 1180 g; column, 9 cm × 70 cm) using a gradient solvent system of petroleum ether/acetone (ratios of 100 ∶ 0, 100 ∶ 2, 100 ∶ 4, 100 ∶ 6, 100 ∶ 8, 100 ∶ 11, 100 ∶ 16, 100 ∶ 22, 100 ∶ 31, and 100 ∶ 41, with 21 L for each gradient elution), to afford ten fractions (F_1–F_{10}) based on TLC analysis. Fraction F_2 was further processed using medium-pressure liquid chromatography (MPLC) with an octadecylsilane (ODS) system, eluting with a gradient of 58%–87% MeOH in H_2O, resulting in seven subfractions ($F_{2\text{-}1}$–$F_{2\text{-}7}$). Purification of subfraction $F_{2\text{-}5}$ (92% MeOH in H_2O) by high-performance liquid chromatography (HPLC) (YMC-pack ODS-AM, 5 μm, 20 mm × 250 mm) yielded compound **1** (t_R 38 min, 10.1 mg). Fraction F_3 was also subjected to MPLC, yielding nine subfractions $F_{3\text{-}1}$–$F_{3\text{-}9}$. Further purification of subfraction $F_{3\text{-}4}$ using MeOH–H_2O (85 ∶ 15) as the mobile phase yielded compound **2** (t_R 41 min, 8.3 mg). Fractions F_7 and F_8 were processed using MPLC with a gradient of 62%–91% MeOH in H_2O, yielding subfractions $F_{7\text{-}1}$–$F_{7\text{-}9}$ and $F_{8\text{-}1}$–$F_{8\text{-}6}$, respectively. Purification of these subfractions by preparative HPLC resulted in the isolation of compound **3** (t_R 37 min, 14.8 mg) from subfraction $F_{7\text{-}3}$ (80% MeOH in H_2O). Fraction F_4 was processed by MPLC using a gradient of 68%–94% MeOH in H_2O, yielding nine subfractions ($F_{4\text{-}1}$–$F_{4\text{-}9}$). Subsequent purification of subfraction $F_{4\text{-}3}$ by HPLC (80% MeOH in H_2O) resulted in the isolation of compounds **4** (t_R 36 min, 5.0 mg),

7 (t_R 41 min, 11.3 mg), and **8** (t_R 37 min, 13.5 mg). Similarly, subfraction F_{4-4} (83% MeOH in H_2O) was purified by HPLC to yield compound **5** (t_R 43 min, 9.2 mg). Additionally, subfractions F_{4-7} and F_{4-8} were combined and further purified by preparative HPLC using 89% MeOH in H_2O, resulting in the isolation of compound 6 (t_R 38 min, 13.4 mg).

*Caseaveolen A (**1**)*: colorless oil; $[\alpha]_D^{20}$ + 17.2 (*c* 0.1, CH_2Cl_2); ECD (CH_3CN) 213 ($\Delta\varepsilon$ + 0.76), 243 ($\Delta\varepsilon$ −0.30) nm; IR (KBr) ν_{max} 2961, 2927, 2876, 1751, 1731, 1457, 1375, 1232, 1051, 960 cm^{-1}; ^1H NMR (400 MHz, $CDCl_3$) and ^{13}C NMR (100 MHz, $CDCl_3$) data, see Tables 1 and 2; HR-ESI-MS *m/z* 527.2988 [M + Na] $^+$ (Calcd. for $C_{29}H_{44}NaO_7$, 527.2985).

*Caseaveolen B (**2**)*: colorless oil; $[\alpha]_D^{20}$ +2.5 (*c* 0.1, CH_2Cl_2); ECD (CH_3CN) 210 ($\Delta\varepsilon$ +1.01), 236 ($\Delta\varepsilon$ −0.71) nm; IR (KBr) ν_{max} 2956, 2927, 2877, 1734, 1457, 1373, 1232, 1051, 959, 898 cm^{-1}; ^1H NMR (400 MHz, $CDCl_3$) and ^{13}C NMR (100 MHz, $CDCl_3$) data, see Tables 1 and 2; HR-ESI-MS *m/z* 485.2517 $[M + Na]^+$ (Calcd. for $C_{26}H_{38}NaO_7$, 485.2515).

*Caseaveolen C (**3**)*: colorless oil; $[\alpha]_D^{20}$ +15.0 (*c* 0.1, CH_2Cl_2); ECD (CH_3CN) 212 ($\Delta\varepsilon$ +0.95), 231 ($\Delta\varepsilon$ −0.83) nm; IR (KBr) ν_{max} 3462, 2957, 2926, 1734, 1456, 1373, 1232, 1050, 1022, 957 cm^{-1}; ^1H NMR (400 MHz, $CDCl_3$) and ^{13}C NMR (100 MHz, $CDCl_3$) data, see Tables 1 and 2; HR-ESI-MS *m/z* 501.2462 $[M + Na]^+$ (Calcd. for $C_{26}H_{38}NaO_8$, 501.2464).

*Caseaveolen D (**4**)*: colorless oil; $[\alpha]_D^{20}$ −53.9 (*c* 0.1, CH_2Cl_2); ECD (CH_3CN) 214 ($\Delta\varepsilon$ +1.04), 292 ($\Delta\varepsilon$ −4.06) nm; IR (KBr) ν_{max} 2956, 2926, 2870, 1751, 1716, 1457, 1375, 1228, 985, 955, 935 cm^{-1}; ^1H NMR (400 MHz, $CDCl_3$) and ^{13}C NMR (100 MHz, $CDCl_3$) data, see Tables 1 and 2; HR-ESI-MS *m/z* 419.2434 $[M + H]^+$ (Calcd. for $C_{24}H_{35}O_6$, 419.2434).

*Caseaveolen E (**5**)*: colorless oil; $[\alpha]_D^{20}$ −31.7 (*c* 0.1, CH_2Cl_2); ECD (CH_3CN) 196 ($\Delta\varepsilon$ −7.25), 213 ($\Delta\varepsilon$ –3.61) nm; IR (KBr) ν_{max} 3482, 2963, 2927, 1732, 1457, 1374, 1225, 1197, 1127, 1041, 947 cm^{-1}; ^1H NMR (400 MHz, $CDCl_3$) and ^{13}C NMR (100 MHz, $CDCl_3$) data, see Tables 1 and 2; HR-ESI-MS *m/z* 499.2672 $[M + Na]^+$ (Calcd. for $C_{27}H_{40}NaO_7$, 499.2672).

*Caseaveolen F (**6**)*: colorless oil; $[\alpha]_D^{20}$ −4.3 (*c* 0.1, CH_2Cl_2); ECD (CH_3CN) 202 ($\Delta\varepsilon$ –7.96) nm; IR (KBr) ν_{max} 3448, 2963, 2929, 1731, 1458, 1374, 1224, 1127, 958 cm^{-1}; ^1H NMR (400 MHz, $CDCl_3$) and ^{13}C NMR (100 MHz, $CDCl_3$) data, see Tables 1 and 2; HR-ESI-MS *m/z* 513.2823 $[M + Na]^+$ (Calcd. for $C_{28}H_{42}NaO_7$, 513.2828).

*Caseaveolen G (**7**)*: colorless oil; $[\alpha]_D^{20}$ −84.8 (*c* 0.1, CH_2Cl_2); ECD (CH_3CN) 200 ($\Delta\varepsilon$ −5.55), 222 ($\Delta\varepsilon$ −3.70) nm; IR (KBr) ν_{max} 3456, 2959, 2928, 1738, 1455, 1372, 1232, 1127, 1022, 949 cm^{-1}; ^1H NMR (400 MHz, $CDCl_3$) and ^{13}C NMR (100 MHz, $CDCl_3$) data, see Tables 1 and 2; HR-ESI-MS *m/z* 471.2354 $[M + Na]^+$ (Calcd. for $C_{25}H_{36}NaO_7$, 471.2359).

*Caseaveolen H (**8**)*: colorless oil; $[\alpha]_D^{20}$ −64.3 (*c* 0.1, CH_2Cl_2); ECD (CH_3CN) 207 ($\Delta\varepsilon$ +5.00), 238 ($\Delta\varepsilon$ −11.97) nm; IR (KBr) ν_{max} 2954, 2926, 2870, 1757, 1676, 1457, 1374, 1222, 1066, 1027, 993, 957, 936 cm^{-1}; ^1H NMR (400 MHz, $CDCl_3$) and ^{13}C NMR (100 MHz, $CDCl_3$) data, see Tables 1 and 2; HR-ESI-MS *m/z* 439.2091 $[M + Na]^+$ (Calcd. for $C_{24}H_{32}NaO_6$, 439.2097).

Computational methods

The ECD spectra calculations were performed as previously described [10, 19]. Detailed methodologies are provided in the Supporting Information.

Cytotoxic activity assay

Cytotoxic activities were evaluated using the MTT assay, following the protocols outlined in previous studies [17, 28]. The detailed experimental procedures for the cytotoxicity evaluation are included in the Supporting Information.

SPR assay

The binding kinetics between compound **8** and VEGFR-2 were analyzed using a Biacore T200 optical biosensor (GE Healthcare, Stockholm, Sweden). The VEGFR-2 protein was immobilized on a CM5 sensor chip using the standard amine coupling method. To determine the dissociation constant K_D, compound **8** was introduced at increasing concentrations (6.25, 12.5, 25, 50, 100, and 200 μmol·L^{-1}). All experiments were conducted in an HBSEP running buffer (pH 7.4).

Molecular docking simulation

Molecular docking simulations were performed using AutoDock Vina software and AutoDock Tools (ADT 1.5.6) with the Lamarckian Genetic Algorithm (LGA) [29, 30]. Detailed experimental procedures are provided in the Supplementary Data.

In vivo antiangiogenetic assay

The anti-angiogenesis activity of compound **8** was evaluated using a transgenic zebrafish *Tg* (*fli1:EGFP*) model, as described in previous studies [31, 32]. Detailed experimental procedures are provided in the Supplementary Data.

In vivo antitumor assay in zebrafish xenografts

The *in vivo* antitumor effects of compound **8** were assessed using a zebrafish xenograft model, following methods previously reported by our team [31, 33]. Detailed experimental methods are provided in the Supplementary Data.

Supplementary Data

Supplementary data can be requested by sending E-mail to the corresponding authors

References

[1] Al-Ostoot FH, Salah S, Khamees HA, *et al*. Tumor angiogenesis: current challenges and therapeutic opportunities [J]. *Cancer Treat Res Commun*, 2021, **28**: 100422.

[2] Hicklin DJ, Ellis LM. Role of the vascular endothelial growth factor pathway in tumor growth and angiogenesis [J]. *J Clin Oncol*, 2005, **23**(5): 1011-1027.

[3] Liu Y, Li Y, Wang Y, *et al*. Recent progress on vascular endothelial growth factor receptor inhibitors with dual targeting capabilities for tumor therapy [J]. *J Hematol Oncol*, 2022, **15**(1): 1-28.

[4] Modi SJ, Kulkarni VM. Vascular endothelial growth factor re-

ceptor (VEGFR-2)/KDR inhibitors: medicinal chemistry perspective [J]. *Med Drug Discov*, 2019, **2**: 100009.
[5] Kinghorn AD, Carcache De BEJ, Chai HB, *et al*. Discovery of anticancer agents of diverse natural origin [J]. *Pure Appl Chem*, 2009, **81**(6): 1051-1063.
[6] Newman DJ, Cragg GM. Natural products as sources of new drugs from 1981 to 2014 [J]. *J Nat Prod*, 2016, **79**(3): 629-661.
[7] Xia L, Guo Q, Tu P, *et al*. The genus *Casearia*: a phytochemical and pharmacological overview [J]. *Phytochem Rev*, 2015, **14**(1): 99-135.
[8] Editorial Committee of the Flora of China, Chinese Academy of Sciences. *Flora of China* [M]. Beijing Science and Technology Press, 1999, **52**(1): 79-80.
[9] Williams RB, Norris A, Miller JS, *et al*. Cytotoxic clerodane diterpenoids and their hydrolysis products from *Casearia nigrescens* from the rainforest of Madagascar [J]. *J Nat Prod*, 2007, **70**(2): 206-209.
[10] Ma J, Yang X, Zhang Q, *et al*. Cytotoxic clerodane diterpenoids from the leaves of *Casearia kurzii* [J]. *Bioorg Chem*, 2019, **85**: 558-567.
[11] Oberlies NH, Burgess JP, Navarro HA, *et al*. Novel bioactive clerodane diterpenoids from the leaves and twigs of *Casearia sylvestris* [J]. *J Nat Prod*, 2002, **65**(2): 95-99.
[12] Oda FB, Crevelin EJ, Crotti AEM, *et al*. Acidic and hepatic derivatives of bioactive clerodane diterpenes casearins J and O [J]. *Fitoterapia*, 2019, **137**: 104197.
[13] Nguyen HTT, Truong NB, Doan HTM, *et al*. Cytotoxic clerodane diterpenoids from the leaves of *Casearia grewiifolia* [J]. *J Nat Prod*, 2015, **78**(11): 2726-2730.
[14] Sai PCV, Hoch JM, Kingston DGI. Structure and stereochemistry of new cytotoxic clerodane diterpenoids from the bark of *Casearia lucida* from the Madagascar rainforest [J]. *J Nat Prod*, 2002, **65**(2): 100-107.
[15] Hunter MS, Corley DG, Carron CP, *et al*. Four new clerodane diterpenes from the leaves of *Casearia guianensis* which inhibit the interaction of leukocyte function antigen 1 with intercellular adhesion molecule 1 [J]. *J Nat Prod*, 1997, **60**(9): 894-899.
[16] Meesakul P, Ritthiwigrom T, Cheenpracha S, *et al*. A new cytotoxic clerodane diterpene from *Casearia graveolens* twigs [J]. *Nat Prod Commun*, 2016, **11**(1): 13-15.
[17] Li Y, Ma J, Song Z, *et al*. The antitumor activity and mechanism of a natural diterpenoid from *Casearia graveolens* [J]. *Front Oncol*, 2021, **11**: 688195.
[18] Liu F, Ma J, Shi Z, *et al*. Clerodane diterpenoids isolated from the leaves of *Casearia graveolens* [J]. *J Nat Prod*, 2020, **83**(1): 36-44.
[19] Xu J, Ji F, Sun X, *et al*. Characterization and biological evaluation of diterpenoids from *Casearia graveolens* [J]. *J Nat Prod*, 2015, **78**(11): 2648-2656.
[20] Beutler JA, McCall KL, Herbert K, *et al*. Novel cytotoxic diterpenes from *Casearia arborea* [J]. *J Nat Prod*, 2000, **63**(5): 657-661.
[21] Whitson EL, Thomas CL, Henrich CJ, *et al*. Clerodane diterpenes from *Casearia arguta* that act as synergistic TRAIL sensitizers [J]. *J Nat Prod*, 2010, **73**(12): 2013-2018.
[22] Liang Y, Zhang Q, Yang X, *et al*. Diterpenoids from the leaves of *Casearia kurzii* showing cytotoxic activities [J]. *Bioorg Chem*, 2020, **98**: 103741.
[23] Mándi A, Kurtán T. Applications of OR/ECD/VCD to the structure elucidation of natural products [J]. *Nat Prod Rep*, 2019, **36**(6): 889-918.
[24] Li XC, Ferreira D, Ding Y. Determination of absolute configuration of natural products: theoretical calculation of electronic circular dichroism as a tool [J]. *Curr Org Chem*, 2010, **14**(16): 1678-1697.
[25] Lv Y, Wang Y, Zheng X, *et al*. Reveal the interaction mechanism of five old drugs targeting VEGFR2 through computational simulations [J]. *J Mol Graph Model*, 2020, **96**: 107538.
[26] Al-Abd AM, Alamoudi AJ, Abdel-Naim AB, *et al*. Anti-angiogenetic agents for the treatment of solid tumors: potential pathways, therapy and current strategies–a review [J]. *J Adv Res*, 2017, **8**(6): 591-605.
[27] Lee D, Yu JS, Ha JW, *et al*. Antitumor potential of withanolide glycosides from Ashwagandha (*Withania somnifera*) on apoptosis of human hepatocellular carcinoma cells and tube formation in human umbilical vein endothelial cells [J]. *Antioxidants*, 2022, **11**(9): 1761.
[28] Lee C, Lee JW, Jin Q, *et al*. Isolation and characterization of dammarane-type saponins from *Gynostemma pentaphyllum* and their inhibitory effects on IL-6-induced STAT3 activation [J]. *J Nat Prod*, 2015, **78**(5): 971-976.
[29] Morris GM, Huey R, Lindstrom W, *et al*. AutoDock4 and AutoDockTools4: automated docking with selective receptor flexibility [J]. *J Comput Chem*, 2009, **30**(16): 2785-2791.
[30] Trott O, Olson AJ. AutoDock Vina: improving the speed and accuracy of docking with a new scoring function, efficient optimization, and multithreading [J]. *J Comput Chem*, 2010, **31**(2): 455-461.
[31] Wang S, Zhang Q, Peng M, *et al*. Design, synthesis, biological evaluation, and preliminary mechanistic study of a novel mitochondrial-targeted xanthone [J]. *Molecules*, 2023, **28**(3): 1016.
[32] Zhang S, Li Y, Li Z, *et al*. Structure, antitumor activity, and potential antitumor mechanism of a fungus polysaccharide from *Fomes officinalis* [J]. *Carbohydr Polym*, 2022, **295**: 119794.
[33] Zhao Y, Zhang X, Li Y, *et al*. A natural xanthone suppresses lung cancer growth and metastasis by targeting STAT3 and FAK signaling pathways [J]. *Phytomedicine*, 2022, **102**: 154118.

Cite this article as: WANG Sibei, LIU Yuhui, LIANG Yue, *et al*. Discovery of antitumor diterpenoids from *Casearia graveolens* targeting VEGFR-2 to inhibit angiogenesis [J]. *Chin J Nat Med*, 2024, **22**(9): 842-853.